Analysis of factors affecting evapotranspiration zoning

Article *in* Environmental Science and Pollution Research · June 2024

DOI: 10.1007/s11356-024-33822-9

4 authors:

Mostafa Sadeghzadeh
University of Tabriz
2 PUBLICATIONS **1** CITATION
SEE PROFILE

Jalal Shiri
University of Tabriz
164 PUBLICATIONS **6,904** CITATIONS
SEE PROFILE

Sepideh Karimi
University of Tabriz
35 PUBLICATIONS **837** CITATIONS
SEE PROFILE

Abolfazl Majnooni-Heris
University of Tabriz
86 PUBLICATIONS **386** CITATIONS
SEE PROFILE

Environmental Science and Pollution Research
https://doi.org/10.1007/s11356-024-33822-9

RESEARCH ARTICLE

Analysis of factors affecting evapotranspiration zoning

Mostafa Sadeghzadeh[1] · Jalal shiri[1,2] · Sepideh Karimi[1,2] · Abolfazl Majnooni[1,2]

Received: 6 March 2024 / Accepted: 22 May 2024

Abstract

Reference evapotranspiration (ET_o) has a significant role in water resource planning and management as well as analysis of crop production and other agricultural tasks. Methods for estimating ET_o may require diurnal/monthly assessments to perceive the consequences of climatic changes on local regions. The spatial and temporal patterns of ET_o were analyzed in the current work using data from 340 weather stations in Iran. The entropy theory was used to assess the uncertainty of the utilized variables and the modified Kendall test was applied for temporal trend analysis. The interpolation (e.g., kriging) and ordinary least squares (OLS) methods were used for spatio-temporal ET_o classification/modeling. The spatial analysis demonstrated that the OLS method with a good fit measure ($R^2 = 0.985$) successfully simulated the spatial relationships of ET_o with climatic parameters. After examining error indices, the cokriging method with an exponential variogram was introduced as the best method of seasonal and annual ET_o classification in Iran. Spatially and temporally calculated ET_o patterns using modified Hargreaves (MHGR) and MODIS methods closely resembled the standard FAO Penman–Monteith (FPM-56) method, all indicating a gradual increase in ET_o. MHGR and MODIS methods serve as suitable alternatives for estimating ET_o in various climatic regions of Iran, provided data availability.

Keywords Entropy theory · FAO Penman–Monteith · Machine learning · Modified Mann–Kendall · Reference evapotranspiration · Zoning

Introduction

The rising temperature, drought, and decreasing land availability have made water crisis for humanity. Evaporation and transpiration, as links between the water and surface energy balance (Lu et al. 2020), are important indicators reflecting climate variations and hydrological processes (Maeda et al. 2011; Kun et al. 2012). Meanwhile, reference evapotranspiration (ET_o) is defined as the maximum quantity of ET from a hypothetical reference surface (grass cover) under specific meteorological conditions, assuming sufficient water availability (Allen et al. 1998). Although the global temperature has increased over the past 50 years, it has been observed that ET_o reacts differently in various geographic regions. For instance, while ET_o has increased in Mediterranean countries and Central Asia (Dadaser-Celik et al. 2015; Vicente-Serrano et al. 2015), it has presented somewhat decreasing trends in Canada (Burn and Hesch 2007), USA (Lawrimore and Petersonm 2000), Australia (Schuur et al. 2015), India (Goyal 2004), and some areas in China (Liu and Zhang 2011; Zheng and Wang 2015). Despite some large-scale studies on ET_o, quantitative studies examining its spatial and temporal trends in regions with varying elevations and latitudes vulnerable to future temperature changes are limited. Since global temperature is expected to rise in the future century (IPCC 2014), understanding spatial and temporal ET_o variations in regions with different climates, elevations, and latitudes is vital. Further, it is particularly essential for analyzing future water requirements of irrigation in regions with water scarcity. In general, the direct effects of climate changes on water resources have been explored via ET_o. Hydrological changes in tropical regions have significant effects on climate changes, and as a result, climate variations will increase temperature values and change the initial precipitation patterns. On the other hand, high temperature values affect the hydrological system and water resources, leading to

Responsible Editor: Marcus Schulz

✉ Jalal shiri
j_shiri2005@yahoo.com

[1] Department of Water Engineering; Faculty of Agriculture, University of Tabriz, Tabriz, Iran

[2] Water Engineering and Science Research Institute (WESRI), University of Tabriz, Tabriz, Iran

Published online: 13 June 2024

increased ET_o (Shahid 2011). Burn and Hesch (2007) identified that changes in precipitation, ET_o, and water scarcity are consequences of public intervention in climate changes. Based on the previously published literature, climate change, which is called as an environmental challenge, increases the rate of ET_o by increasing the temperature in a region. Since many regions of Iran are subject to dry climatic conditions, the resulting climate changes will directly affect the agricultural activities of the region in the future, causing disruptions in the availability of water. As there was no comprehensive study focusing on relations between the climate change and ET_o variations, the present research focused on evaluating the factors affecting the spatial and temporal changes of ET_o. Considering numerous factors that influence ET_o variations, the temporal and spatial differences between ET_o variations and climatic change are complex and diverse. Moreover, it is not yet clear to what extent changes in ET_o are driven by specific factors. Therefore, a proper assessment of ET_o and its potential changes due to climate variations is necessary for water resource planning and management. The objectives of the present study are as follows:

1. To analyze the spatiotemporal trends, transformation features and regional heterogeneity of ET_o across Iran.
2. To identify the key influential variables on ET_o through entropy theory and deriving it using machine learning methods and geographic information systems.
3. Investigating the spatiotemporal features of ET_o and quantifying it at different elevations and geographical latitudes.
4. To identify the leading climatic basis affecting ET_o changes at different stages.
5. Providing a method to identify data gaps at weather stations.
6. Introducing a new approach for ET_o estimation that considers climate, geographical latitude, and more.

Materials and methods

Study area

Data from 340 weather stations across Iran were utilized (Fig. 1). The climatic contexts of the studied regions have been identified based on aridity index (UNEP, 1992). The stations with the higher elevations have arid and semi-arid climate, while the stations with lower elevations is located in very humid and humid climate. ET_o estimation was performed using daily records of maximum relative humidity (RH_{max}), minimum relative humidity (RH_{min}), maximum air temperature (T_{max}), minimum air temperature (T_{min}), solar radiation (R_s), and wind speed (W_s) for each station over an 11-year period (2011 to 2021). Through the utilization of the entropy package in R software, an analysis is conducted to identify the primary factor contributing to variations in ET. Subsequently, Modis images are employed, along with the amalgamation of climate maps, to undertake zoning and validate the optimal model within GIS software.

Models used for ET_o estimation

Penman–Monteith equation adopted by FAO (FPM-56) is the commonly used method of ET_o estimation under

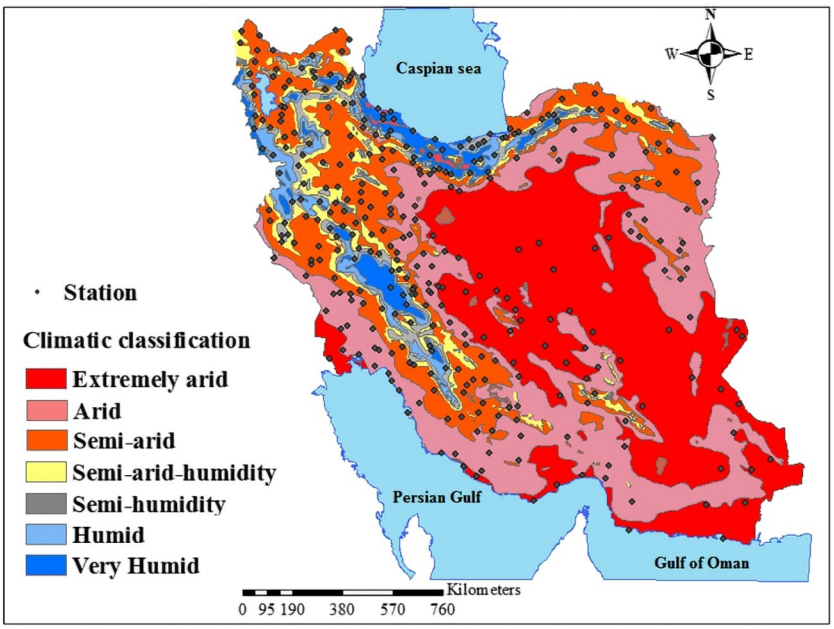

Fig. 1 Localization of the study area

full data availability conditions. FPM-56 was used here as the benchmark model and other methods relying on fewer input parameters were employed for comparing with FPM-56 to assess their accuracy and capability. As a common temperature-based model, Hargreaves-Samani and its modified version was used that can be easily applied when available weather data are limited. The temperature-based Blaney-Criddle method (BCR) was also applied due to its extensive global applications in assessing climate changes (Zhang et al. 2022). The mass transfer-based Dalton method was utilized to assess the context of the models that use the aerodynamic fundamentals of transfer (Shiri 2018). Finally, the MODIS (Moderate Resolution Imaging Spectroradiometer) images were used, assuming that ground-based data are unavailable.

FAO-56 Penman–Monteith Model

The FPM-56 model is a modified version, replacing the original Penman model (Penman 1948) that has merit in handling bulk surface resistance (r_s) and aerodynamic resistance (r_a). Combining the mentioned terms, the original Penman method estimates ET_o from the surface vegetation cover accurately. Additionally, the model can be adjusted for specific types of vegetation cover. This model has been certified as the benchmark method universally (Chu et al. 2017; Jhajharia et al. 2012). Allen et al. (2007) modified the fundamental equation of FPM-56, considering the coefficients of variables mathematically as:

$$ET_{0=}\frac{0.408\Delta\left(R_n-G\right)+\gamma\frac{900}{T+273}u_{2(e_s-e_s)}}{\Delta+\gamma(1+0.34u_2)} \quad (1)$$

In which ET_o represents the reference evapotranspiration (mm day^{-1}), R_n is the solar net radiation at the surface of vegetation cover (MJ m^{-2} day^{-1}), G shows the soil heat flux (MJ m^{-2} day^{-1}), T is the average air temperature at two meters above the ground surface (°C), u_2 is the wind speed at 2 m above the ground surface (m s^{-1}), ea is the actual vapor pressure (kPa), es is the saturated vapor pressure (kPa), es − ea is the vapor pressure deficit (kPa), Δ is the slope of the vapor pressure curve (kPa °C^{-1}), and γ is the psychrometric constant (kPa °C^{-1}).

Mass transfer–based model

Aerodynamic (mass transfer) methods follow Dalton's law that evaporates from the surface into the atmosphere and describe turbulent transport of water vapor (Shiri 2019). These are simple methods that can be used when there is a lack of sunshine duration data. For free water surface, these models can be written as (Bogawski and Bednorz 2014):

$$E=a_{mt}(b_{mt}+c_{mt}u_2)(e_w-e_d) \quad (2)$$

where a_{mt}, b_{mt}, and c_{mt} are constants and e_d and e_w are the actual and saturate vapour pressure at water surface (kPa). So, the model can be written as (Gianniou and Antonopoulos 2007):

$$ET_0=2.032\left(1+0.26u_2\right)(e_w-e_d) \quad (3)$$

where ET_o is expressed in mm day^{-1}, e_w and e_d in kPa, and u_2 is in ms^{-1}.

Hargreaves-Samani model

Hargreaves and Samani (1985) model is a suitable and convenient model of ET_o estimation in different climate locations:

$$ET_{HGR}=0.00233*R_a*\left(T_{max}-T_{min}\right)^{0.5}\left(\frac{T_{max}+T_{mim}}{2}+17.8\right) \quad (4)$$

An exponentially calibrated version of this model (MHGR) was used here as follows (Subburayan et al. 2011):

$$ET_{HGR}=0.00233*R_a*\left(T_{max}-T_{min}\right)^{0.213}\left(\frac{T_{max}+T_{mim}}{2}+17.8\right) \quad (5)$$

By using this version, Hargreaves-Samani model (HGR) tendency for overestimation in humid regions will be reduced considerably (Subburayan et al. 2011).

Blaney-Criddle model

The temperature-based Blaney and Criddle (1950) model was developed to predict ET_o (Doorenbos and Pruitt, 1977), which is presented below:

$$ET_O=P*(0.46*T+8.13) \quad (6)$$

where T = mean air temperature (°C) and P = the number of daylight hours on a given day as a percentage of the total number of daylight hours in a year (%.), which is obtained from the table.

MODIS images

There are plenty of approaches for spatial extrapolation of ET on the basis of remotely sensed observations (Glen et al., 2008; Li et al., 2009). These strategies can be categorized in two main groups:

1. Physics-based methods, which utilize remote sensing surface temperature and surface energy balance analysis

or biophysical surface properties like the Penman–Monteith equation (Bastiaanssen 2000; Mu et al. 2011).
2. Regression methods, where an empirical relation is directly applied between remotely sensed vegetation indices and observed ET (Glenn, 2010).

In the long term, it has been accepted that physics-based ET methods will prevail because of their strong theoretical foundation, so they can provide accurate extrapolation of ET with precise representation of the surface. However, in the short term, physics-based approaches may be limited in mountainous areas and regions with limited meteorological stations (Goulden et al. 2012). Physics-based approaches require detailed meteorological inputs, which can be challenging to extrapolate accurately in mountainous areas due to heterogeneity and limited data. Soil properties also vary with topography, making conditions in mountain areas unique (Goulden et al. 2012).

When comparing the second group, regression techniques rely only on remotely sensed vegetation indices and are less affected by the lack of precise weather and soil information. However, the assumption that physics-based strategies are superior to regression approaches is challenged by several considerations. Overall, while ET algorithms are constraint functions, complex approaches do not always outperform simpler regression strategies (Beven 2006).

Artificial neural network

Artificial neural networks (ANNs) are derived from biological neural networks that are able to process information quickly and identify patterns to adjustment solutions over time (Jain, 2008). As there is no unique method for selecting the convenient architecture of the ANN (Wu et al. 2014; Coulibaly et al. 2001), the trial and error method was used to identify the number of neurons in the hidden layers. This method showed that when the number of neurons ranged from 5 to 8 in the hidden layer, similar results were obtained. Here, five input variables were used, including solar radiation, minimum and maximum air temperature, wind speed, and relative humidity through different input combinations, as will be explained in the next sections.

Before passing the neural network, in order to avoid too small weight factors and convergence problems, it is better to standardize all input and output values, especially when the data size is large. In this study, the following equation was used to normalize the variables:

$$x_{ni} = \frac{x_i - x_{min}}{x_{max} - x_{min}} \tag{7}$$

where x_{ni} is the normalized dimensionless variable; x_i is the observed value; $x_{\min}$ and $x_{\max}$ are the minimum and the maximum observed values. For establishing the ANN models, all available patterns were divided into training (70%), testing (20%), and validation (10%) phases. Back propagation forward feed forward neural network with Levenberg–Marquardt training algorithm was implemented. A gradient descent with momentum and adaptive learning rate was used as an adaptive function and the sigmoid function was used as the activation transfer function.

Investigating factors affecting ET_o

Shannon's entropy theory

Derived from information theory, Shannon's entropy model was first introduced by Claude E. Shannon in 1948 and is a measure of disorder in a system (Bednarik 2010). Entropy is classified into two categories, namely, discrete and continuous. In the latter case, it is assumed that the probability distribution of variables follows a normal or log-normal distribution, while in the first case, the information is discretized and frequency distribution tables of variable observations are created based on the range of variable values. Then, the probability values of events occurring in each case are calculated using these tables. Therefore, the type of probability density function is not important. Recent studies have shown that many quantitative and qualitative variables in water resource systems do not follow a normal or log-normal distribution (e.g., Moghier and Singh 2003). Thus, using discrete entropy is a way to address this significant drawback in entropy applications. Accordingly, discrete boundary entropy was used in the present study and the amount of transfer entropy from input variables to the target variable (ET_o) was calculated.

Shannon and Weaver (1949) presented the boundary entropy, $H(x)$, from a discrete random variable x as:

$$H(x) = -k \sum_{i=1}^{n} P(x_i) \log P(x_i) \tag{8}$$

One can consider $k=1$ if $H(x)$ is expressed in the Naper unit based on the natural logarithm. n indicates the number of possible events $p(x_i)$ ($i=1,..,n$). Therefore, the following equation is used for identifying the entropy of information transfer:

$$T(x,y) = -\sum_{i=1}^{\infty} \sum_{j=1}^{\infty} P(x_i, y_j) 1n \left[\frac{P(x_i, y_j)}{P(x_i) P(y_j)} \right] \tag{9}$$

In these equations, $P(x)$ represents the probability of event x, and $P(x,y)$ represents the joint probability of events x and y.

Examination of meteorological data trends

Hamed and Rao (1998) introduced the modified Kendall test. By using this method, all significant autocorrelation structures in the time series are examined and removed. The modified variance $V(s)*$ is used in calculating the Mann–Kendall statistic Z as:

$$Var(S) *= Var(S)\frac{n}{n*} \tag{10}$$

$$\frac{n}{n*} = 1 + \frac{2}{n(n-1)(n-2)}\sum_{i=1}^{n-1}(n-i)(n-i-1)(n-i-2)ri \tag{11}$$

in which r_i represents the autocorrelation coefficient with a lag of i, and $Var(S)$ is estimated from the equation. n/n^* represents a correction due to the autocorrelation or effective sample size (n is the actual number of observations and n^* is considered an "effective" number of observations, accounting for the autocorrelation in the data). To compute the Z statistic of the modified Mann–Kendall test in the last equation, $Var(S)$ is replaced with $Var(S)*$. The Z statistic value is compared to the critical value of a normal distribution at a significance level α. If the absolute value of the Z statistic obtained from the non-parametric Mann–Kendall test is greater than 1.64, the trend will be significant at 10% level. If it is greater than or equal to 1.96, the trend will be significant at 5% level, and if it is greater than or equal to 2.58, the trend will be significant at 1% level (Hamed and Rao 1998).

Spatial estimation of ET_o using statistical methods

The inverse distance weighting (IDW), kriging, and cokriging methods were performed to generate predictive maps of ET_o in the present research.

Inverse distance weighting

The IDW method is a widely used approach that has showed the lowest average error in most of spatial analysis cases (e.g., Raziei and Pereira 2013; Chuanyan et al. 2005). The weight assigned to each sample point is proportional to the inverse distance between the sample point and the target location (Tong et al., 2007). Considering the distance D_i between the sample and target points, the value of a single point would be calculated as:

$$M = \frac{\sum_{i-1}^{n} M_i \Big/ (D_i)^2}{\sum_{i-1}^{n} 1 \Big/ (D_i)^2} \tag{12}$$

in which M is the variable estimation value, M_i is the sample value at point i, and D_i is the distance between the sample point and the estimated point.

Kriging method

As a geostatistical method, kriging is basically based on weighted moving average, which has no systematic error and has minimum estimation variance (Dobesch et al., 2007). This method is based on the definition of variogram, and the success of the method depends on choosing the right or optimal variogram model. Variogram is used to calculate weight in kriging method. The variogram is defined as a measure of half variance in term of a distance function:

$$y^{(h)} = \frac{1}{2N(h)}\sum_{i=1}^{N(h)}[z(x_i) - z(x_i+h)]^2 \tag{13}$$

where $\gamma(h)$ is the experimental semivariogram at lag distance h, $N(h)$ is the number of data pairs at lag distance h, $Z(x_i)$ is the measured sample value at position xi, and $Z(x_i+h)$ is the measured sample value at position (x_i+h). Spatial distribution of data is empirically discussed with fitting models. Informational mathematical models on the spatial variability structure and input parameters for kriging are provided. The models were fitted with environmental variables, showing that these variables exhibit spatial autocorrelation within their effective ranges. Linear, exponential, and Gaussian models were used to fit the experimental variogram here.

Ordinary kriging

Ordinary kriging (OK) is an intrinsic spatial statistical method based on the spatial dependence of the response variable used to find the best unbiased linear approximation (Goovaerts 1997). The general form of the OK is:

$$\hat{Z}(x_p) = \sum_{i=1}^{n}\lambda_i Z(x_i) \tag{14}$$

To reach unbiased estimates in OK, the set of equations below must be simultaneously solved:

$$\sum_{i=1}^{n}\lambda_i\gamma(x_i,x_j) - \mu = \gamma(x_i,x_p) \tag{15}$$

in which $j=1,\ldots,n$

$$\sum_{i=1}^{n}\lambda = 1 \tag{16}$$

where $\hat{Z}(x_p)$= the expected value of variable Z (i.e., ET_o) at position x_p, $Z(x_i)$ = the certain value at position x_i, λ_i = the

weights concerted with the data, μ = the Lagrange multiplier, $\gamma(x_i, x_j)$ = the value of the cross-variogram between vectors starting at x_i and ending at x_j, and n = the point estimation involves the use of sample data.

Cokriging method

The cokriging method (CK) estimator is a multivariate equivalent to kriging estimator with covariates. Using different datasets, this is a highly flexible and robust geostatistical gridding method that allows the user to investigate auto-correlation and cross-correlation patterns. The cokriging estimation is introduced with the following equation:

$$\sum_{i=1}^{v}\sum_{i=1}^{n}\lambda_{il}\lambda_{lv}\left(x_i,x_j\right)-\mu_v=\mu_{uv}(x_i,x_p) \tag{17}$$

in which $j = 1,\ldots,n$
And $u = 1,\ldots,v$
With

$$\sum_{i=1}^{nl}\lambda_{il}\begin{cases}1,1=u\\0,1\neq 1u\end{cases}$$

in which u and v are the elementary and secondary data. These two variables are correlated with each other and assist in estimating the primary data.

For the analysis of CK, cross-variograms need to be determined in advance. Cross-variogram models are obtained by fitting them with empirical cross-variograms between elementary and secondary data, calculated using the following equation:

$$\gamma_{uv}(h)=\frac{1}{2N(h)}\sum_{i=1}^{N(h)}\left[z_u\left(x_i\right)-z_u(x_i+h)\right]\left[z_v(x_i)-z_v(x_i+h)\right] \tag{18}$$

To generate predictive maps of ET_o values, various auxiliary variables are used in this present study according to significant correlations between ET_o and climatic parameters, as noted in the next steps.

Estimation of spatial models

Ordinary least squares (OLS) model appertaining to Carl Friedrich Gauss 1809 (Stephen 1981) is one of the most powerful regression analysis methods due to its statistical properties. OLS considers the total of squared differences, along the side of the axis of the dependent variable, between each datum in the dataset and the corresponding point in the regression level. Lower values of differences indicate better fit model on data. The resulting estimator can be considered for a simple linear regression, where the independent factors are on the right side of the equation and the dependent factor is on the left side of the equation.

In this study, OLS regression is used to model the dependent factor (ET_o) in relation to the independent factors (e.g., wind speed, temperature difference, solar radiation, relative humidity, elevation above sea level, and geographical latitude) in the following form:

$$ET_o=f\left(\triangle T,W_s,RH\%,R_s,\ \text{elevation},\ \text{latitude}\right) \tag{19}$$

$$ET_o=a_0+a_1\Delta T+a_2W_S+a_3RH\%+a_4R_s+a_5Altitude+a_6Latitude+e \tag{20}$$

where α_0 is the intercept, and α_1 to α_6 are the estimated coefficients for the independent factors. e denotes the error and ΔT is the difference between maximum and minimum temperature values.

OLS can produce feature class and optional tables with informative vision and easily interpretable coefficients. The following phases were involved in conducting the OLS estimations:

1. Raster maps of all dependent and independent variables were prepared.
2. The independent factors were overlaid and weighted together in the GIS domain. Weighting for each variable was determined based on its effect on ET_o.
3. Residuals value is formed. So, exploratory spatial data analysis was performed on standardized residuals to investigate whether residuals are randomly distributed or not. Spatial autocorrelation in spatial distribution of residuals is also used to recognize whether any of the independent factors are important in the regression. If the regression residual analysis is distributed in a scattered or clustered manner, the model is considered incomplete or biased.

Performance evaluation criteria

Three statistical indices, namely, the root mean square error (RMSE), the correlation coefficient (R), and the scatter index (SI), were utilized for evaluating the models:

$$r=\frac{\sum_{I-1}^{N}(O_i-O_m)^2(C_i-C_m)}{\sqrt{\sum_{i-1}^{N}(O_i-O_m)^2\sum_{i-1}^{N}(C_i-C_m)^2}} \tag{21}$$

$$RMSE=\sqrt{\frac{1}{N}\sum_{i=1}^{N}(C_i-O_i)^2} \tag{22}$$

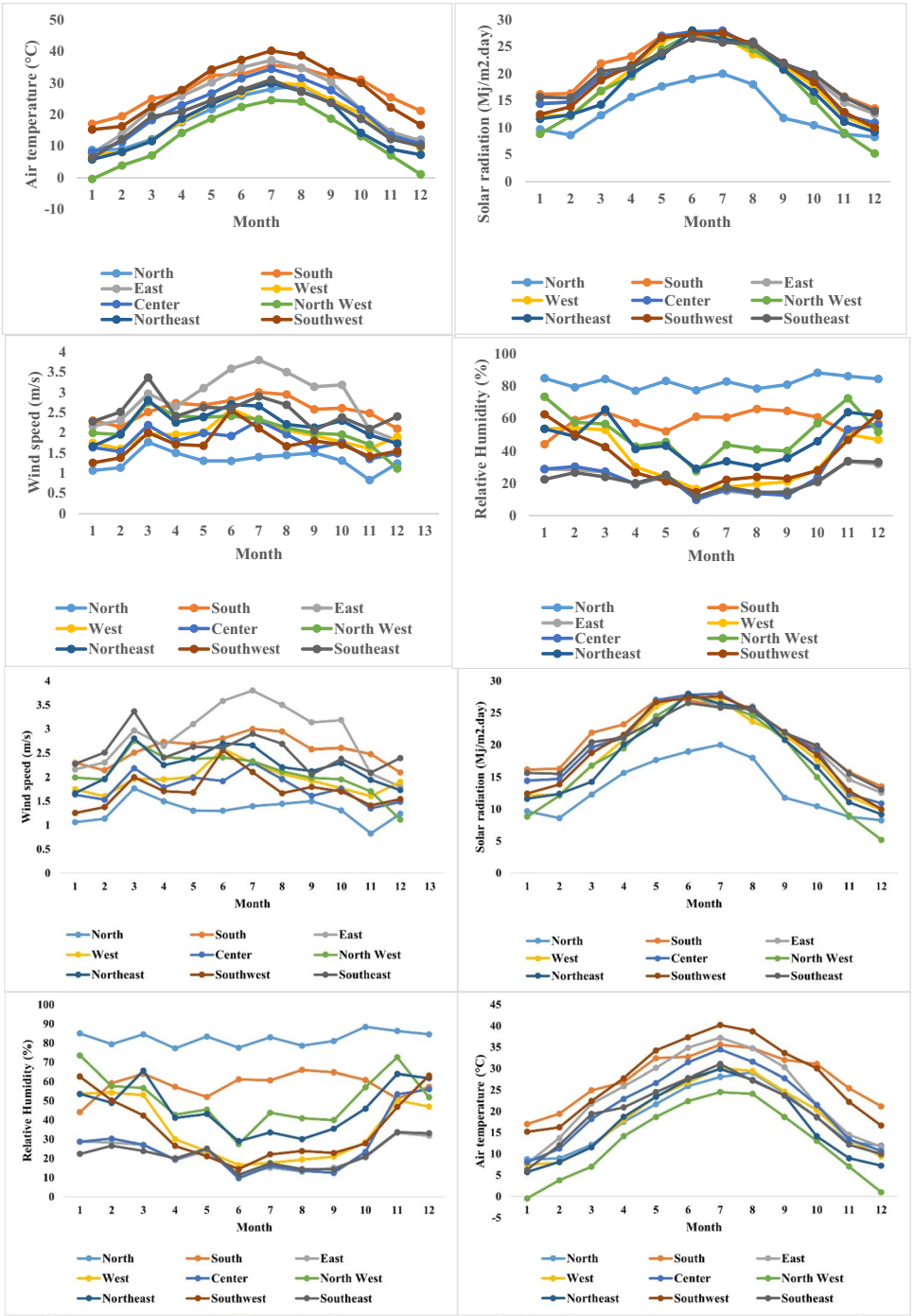

Fig. 2 Monthly average variations of the main meteorological variables

$$SI = \frac{\sqrt{\frac{1}{N}\sum_{i=1}^{N}(C_i - O_i)^2}}{\overline{O}_m} \tag{23}$$

where O represents the ET_o values obtained by PM-56 model, and C represents the calculated ET_o values using other methods. The subscribe "m" refers to the mean values.

Results and discussion

Observations during the study period

Monthly average values of the main meteorological variables are displayed in Fig. 2 for six geographical regions of the study area. Analyzing the plots, it was observed that:

1. monthly variations in relative humidity are greater in the northwestern, northeastern, southwestern, and western regions compared to other areas, which experience relatively minor variations throughout the year. Furthermore, northern and southern regions have the highest humidity during the year, while central, southeastern, and eastern regions exhibit the lowest humidity.
2. The most significant changes in wind speed are observed in the eastern, southeastern, and southern regions, while the northern areas showed the lower variation. Wind speed increases for all regions in March, and seasonal wind speed variations are more obvious in the eastern and southeastern regions.
3. The highest solar radiation values have been recorded during January to May in the southern regions, shifting to June and July in the central region. The most significant seasonal variations in solar radiation are observed in the northwestern regions, while the northern areas exhibit the lowest variations.

Attending the overall ET_o variations, a graphical summary of the annual variability of ET_o in different regions of Iran is presented in Fig. 3. The figure illustrates the cumulative probability of annual variability for different regions of Iran. The range of total ET_o signifies the estimated variability for the growing season in these locations. The highest recorded ET_o (shortest monthly growth season) is observed in the eastern, southeastern, and central regions, which may be partly attributed to local weather conditions. For example, warmer temperatures and stronger winds (refer to the Fig. 2) in these areas may explain this trend. The lowest ET_o (longest monthly growth season) is found in the northern, northwestern, and western regions. This shows that the variability of estimated ET_o during the growing season for these locations is high. The coefficient of variation (CV: the ration between the standard deviation and the mean value of ET_o) can provide valuable insights into the relative variability of data when the average values are subjected to variations. The general variability of ET_o estimates among the stations is illustrated in Fig. 3 in term of CV. A relatively linear increase in ET_o from 2016 to 2021 can be observed there, while from the period between 2011 and 2016 a decreasing trend was experienced. Overall, this trend has been upward over the past decade and it is more obvious in summer season.

Mutual information entropy

Climate indices may provide valuable information on ET_o variability. One may start by analyzing the mutual information (MI) between variables, as summarized in Fig. 4. The values of MI entropy are interpreted as a reduction in uncertainty in target (ET_o) values based on knowledge of a random input variable, so it presents the magnitude of the transferred information from inputs to the target variable. From Fig. 4, MI between daily wind speed and ET_o is significantly lower than the rest of the variables. This may be due to the lower entropy in wind speed data, which has resulted in less MI between these two variables. This is in agreement with the previous studies (e.g., Gong et al. 2006). Further, wind speed showed negative impact in humid regions, while its impact is positive arid and semi-arid regions. Humid areas were less affected by wind speed than arid areas, which might be linked to the higher humidity values in those regions. The effect of wind speed on the amount of ET_o is more obvious for areas with lower relative humidity than the areas with higher relative humidity. Physiologically, the decrease of wind speed impact on ET_o can be justified due to the closing of the stomata under the influence of wind stress in higher wind speed values, which reduces the transpiration rate. Under such situation, the rate of transpiration is no longer dependent on wind

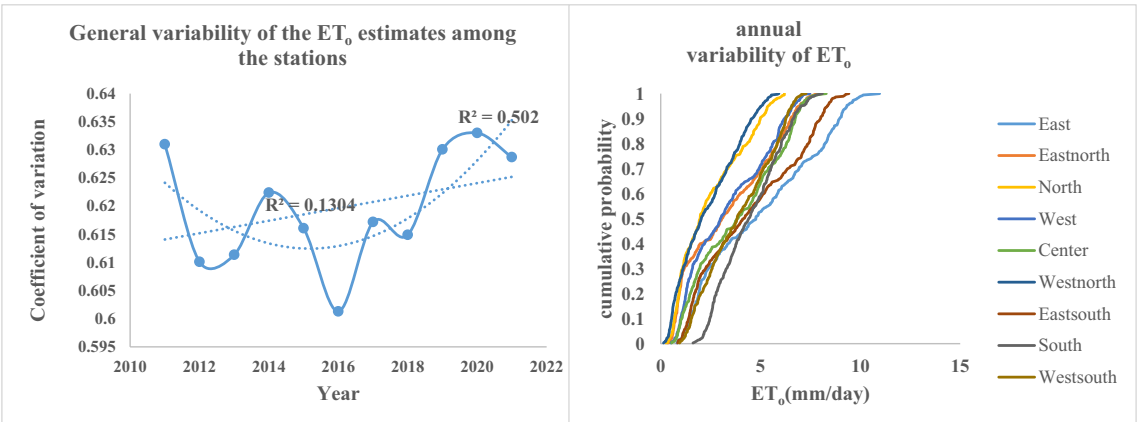

Fig. 3 Overall variability and cumulative probability distribution of ET_o among stations from 2011 to 2021

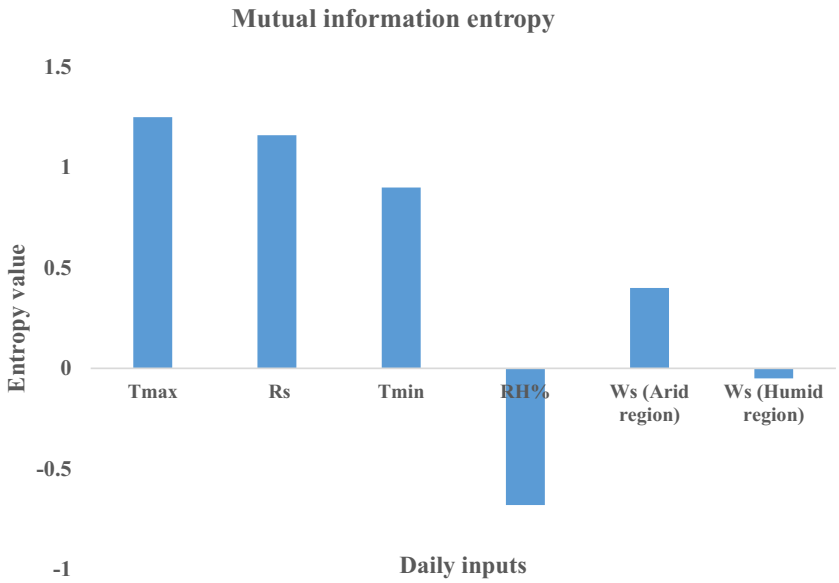

Fig. 4 Received output information from daily input parameters

speed, but is controlled by other meteorological parameters. The maximum MI was corresponded to the maximum air temperature and solar radiation, indicating that these variables share more information with ET_o. This may be somewhat due to higher maximum temperature values compared to other parameters at stations, as well as its attribution in estimating net radiation, saturation vapor pressure, and vapor pressure gradient, as discussed by Irmak et al. (2006), Patle and Singh (2015), and Liu et al. (2014).

Estimation of ET_o

Table 1 summarizes the statistical indices of various ET_o estimation methods. Based on the results, BCR and MHGR gave the better results than the HGR and mass transfer models. Modis method (based on space-born information) surpassed the HGR and mass transfer models for arid and semi-arid locations, respectively. Although comparable results were obtained by using these methods, MHGR model would be recommended as the most accurate model due to its simpler expression that requires limited meteorological data. However, MHGR overestimates the ET_o values in humid locations, while it provides underestimated ET_o values in arid regions, which is in agreement with conclusions obtained by Shiri et al. (2015). Nevertheless, the performance accuracy of Modis method is acceptable when no land and climate information are available. Figure 5 shows a visual illustration of the ET_o values obtained by MHGR and Modis methods vs. the FPM-56 benchmark ET_o values.

Regarding the ANN models, the input matrix consisted of T_{max}, T_{min}, RH%, R_s, and W_s, while ET_o values were the target variable. Both input and target variables were standardized before training and testing the models as explained

Table 1 Comparison of various methods for daily ET_o estimation with the FPM-56 method

Method	Region	R^2	RMSE	SI
HGR	Humid	0.91	6.80	2.50
	Arid and semi-arid	0.86	7.40	2.70
	All	0.84	8.10	3.01
MHGR	Humid	0.94	0.71	0.26
	Arid and semi-arid	0.89	0.85	0.32
	All	0.87	0.92	0.34
BCR	Humid	0.88	0.74	0.27
	Arid and semi-arid	0.87	0.78	0.30
	All	0.85	0.94	0.35
Modis Image	Humid	0.90	1.5	0.55
	Arid and semi-arid	0.94	1.3	0.48
	All	0.88	1.7	0.63
Mass Transfer	Humid	0.87	0.99	0.37
	Arid and semi-arid	0.83	1.2	0.44
	All	0.81	1.4	0.52

before. Based on the results presented for all stations in Table 2, the ANN model fed with all necessary parameters (ANN1) outperformed the rest of the ANN models, while the ANN6 that used only maximum and minimum temperature values as input produced the higher SI values (the lowest comparative accuracy). However, difference between SI values of ANN1 and ANN6 is small ($\Delta SI = 0.08$). Therefore, it is seen that ANN with fewer input parameters can simulate the ET_o values well. Abraham and Mohan (2023) argued that ANN models performed very well in coastal, per-humid, and humid climate regions, but their performance accuracy was slightly poor in warmer regions (Abraham and Mohan 2023), confirming the reported statements. Other researchers

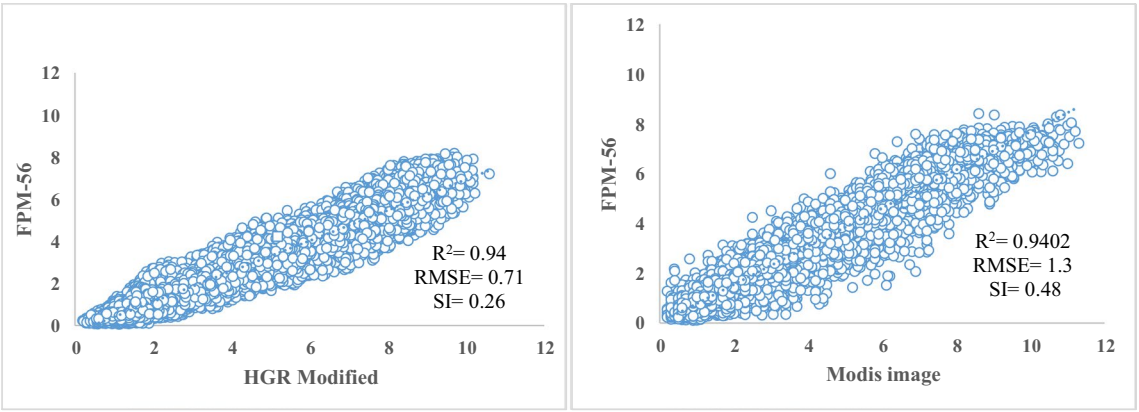

Fig. 5 Scatterplot of daily ET_o estimation for two best methods: MHGR (humid regions) and Modis images (arid and semi-arid regions)

have also employed artificial intelligence methods for estimating ET_o all of which appear to be satisfactory (Shiri et al 2014; Traore et al., 2016).

Spatial interpolation

Three common spatial interpolation methods were tested, and their internal consistency was evaluated using cross-validation. The statistical indices of the interpolated values of ET_o and other meteorological parameters for three best methods are presented in Table 3. The cokriging)with auxiliary parameters of temperature and solar radiation) with exponential variogram method was chosen for interpolating the mean annual and mean seasonal values at 340 stations due to having the highest correlation coefficient and the lowest error compared to other interpolation methods. The variable network results demonstrated that the accuracy of the interpolated outputs, particularly concerning T_{max}, T_{min}, RH%, R_s, and ET_o, is logically high. Higher estimation errors were found for W_s since it is a local dependent variable and significantly influenced by topography.

Spatial distribution of ET_o in seasonal and annual scales

The spatial distribution of annual and seasonal ETo calculated using the cokriging method is depicted in Fig. 6, illustrating the merged influence of available climatic parameters. It demonstrates the seasonal variations of meteorological parameters throughout the study area (refer to Fig. 2), resulting in varying patterns for ETo. The patterns show a gradual increase in west–east and north–south directions. The lowest ETo values are observed in the northern and northwestern humid regions, while the highest values belong to the arid and extremely arid climates in the eastern, central, southern, and southeastern regions. In winter, the lowest values are observed in the northern part of the country, while the highest values are observed in the south and southeast

Table 2 Statistical indices of the ANN models for all stations

Method	Inputs	R^2	RMSE	SI
ANN1	T_{max}, T_{min}, R_s, W_s, RH%	0.99	0.51	0.14
ANN2	T_{max}, T_{min}, R_s, W_s	0.97	0.57	0.16
ANN3	T_{max}, T_{min}, R_s	0.95	0.61	0.17
ANN4	T_{max}, T_{min}, W_s	0.92	0.63	0.18
ANN5	T_{max}, T_{min}, RH%	0.87	0.76	0.21
ANN6	T_{max}, T_{min}	0.86	0.77	0.22

regions. As shown in Fig. 2, higher temperature and solar radiation, low humidity, and high wind speed are the main factors contributing to the high ET_o values in the southern and southeastern regions during the winter season.

In spring, the spatial distribution of ETo is similar to summer, although the differences are less pronounced in most parts of the area. Higher values of ETo are observed in the southeastern and eastern regions, linked to higher wind speed and lower humidity. A clear west-to-east and north-to-south gradient is evident, primarily driven by temperature and solar radiation, while the difference in relative humidity is minimal. ETo has relatively homogeneous spatial distribution during autumn. The annual ETo distribution has relatively small areas in the high-altitude regions in the northwest and east as well as the central part of the basin, with a clear decreasing trend from the low-lying plains to the high-altitude areas.

Combining spatial distributions of ET_o and meteorological variables, land cover, and physical interpolation provides important insights for studies on climate change in the region. Summer ET_o is obviously high in low-lying plains than the high-altitude areas. Spring, summer, and autumn ET_o trend was decreasing when altitude was increased, with greater differences in maximum and minimum temperatures during the warm months compared to the cold months.

Table 3 Comparison of the quality of interpolation

Method	ET_o		R_s		W_s		RH%		T_{min}		T_{max}	
	R^2	RMSE	R^2	RMSE	R^2	RMSE	R^2	RMSE	R^2	RMSE	R^2	RMSE
IDW	0.76	39.1	0.75	0.78	0.15	0.66	0.72	8.7	0.7	2.84	0.77	2.3
Kriging (exponential)	0.79	36.3	0.78	0.73	0.17	0.65	0.8	7.3	0.73	2.6	0.8	2.2
Cokriging (exponential)	0.89	25.7	0.79	0.7	0.45	0.33	0.83	6.6	0.8	2.2	0.86	1.8

Annual trends of ET_o, and key meteorological variables

Figure 7 presents the spatial trend of annual averages of ET_o, R_s, W_s, RH%, T_{max} and T_{min} during the study period, encompassing the entire country during the years 2011–2021. An increasing trend is evident for ET_o, T_{max}, and T_{min} values. The observed temporal trend in Fig. 7 reflects the combined effect of all meteorological variables that shows the positive influence of meteorological variables (except RH% and W_s) on ET_o in the humid regions. Solar radiation provides the necessary energy for water evaporation from the surface of the soil and plants by heating the air passing over the evaporating surface. To perform ET_o, moist air must be removed from the environment, which results in reduced evaporation when moving away from seas to drier grassland and mountainous areas. The trends in each station differ, with most of them showing an increasing trend in annual ET_o. Annual analyses revealed that most points of the studied area exhibited increasing trends accompanied by abrupt changes in the region. The highest increase in annual ET_o was found in the southern, southeastern, and southwestern regions of the country (increasing by up to 2000 mm per year), while the lowest values were in the northern regions (800 mm per year). In general, the results indicate that the southeastern, southwestern, and southern regions of Iran have relatively high ET_o. As the changes in ET_o result from comprehensive effects of climatic variables, it is necessary to analyze each meteorological variable separately over this period. From the investigations, these increases are attributed to rising air temperature, increased solar radiation, and decreased relative humidity in the region. The analysis reveals significant increasing trends in maximum and minimum air temperatures over the past 11 years. The trend is statistically significant at a 5% level of significance. This upward trend is also linked to global temperature rise and reported by Niggli et al. (2009). Regarding the decreasing and increasing trends in solar radiation, the decrease in global solar radiation (duration of solar radiation) might be due to dust, pollution, and cloudy conditions, while the increase may be due to the potentially increasing wind speed in wind corridors and sky clearness in the region. Similar analysis has been reported by Zhang et al. (2014), based on measurements of total global radiation in eastern China. Moreover, Fig. 6 indicates no significant increasing trend for relative humidity except some limited locations. Although relative humidity is one of the most sensitive meteorological variables, its contribution to the upward or downward trend of ET_o is not more obvious, as it does not exhibit a significant overall increase or decrease throughout the area.

Attending to the wind speed variations, local wind speeds are considered a function of the pressure system's position and the region's topography. Wind speed data related to arid areas (eastern, southeastern, southern, and central parts of Iran) indicated much higher values than the humid areas. The higher wind speed in these regions may be attributed to the lower vegetation cover and higher roughness. However, its effect is moderated by air temperatures and relative humidity; e.g., warm and dry air enhances evaporation more than cool and humid air. Nevertheless, wind speed shows an overall increasing gradient from north to south and from west to east. Concerning the relationship between ET_o and wind speed, with the initiation of wind flow (at low wind speeds), an increase in the vapor pressure difference occurs due to the decrease in vapor pressure of the air layer attached to the evaporating surface caused by air displacement, as well as an increase in vapor pressure of the water inside the leaf due to leaf turbulence. This increases the evaporation amount from the leaf area (Irmak and Mutiibwa 2009). Furthermore, as wind speed increases, leaf stomata begin to close physiologically, and the rate of ET increases with lower acceleration, and ultimately, at higher wind speeds, ET reaches a constant value (low slope). So, at higher wind speed values, ET is no longer wind-dependent but is controlled by other meteorological parameters. Therefore, the effect of wind speed on ET_o is more pronounced in regions with low humidity (southeastern, southwestern, southern, and central Iran) compared to regions with higher humidity (northern, northwestern, and eastern Iran). In Fig. 8, the relationship between wind speed and annual ET is plotted for both arid and humid regions. The relationship between the proportional increase of ET_o and W_S is evident for lower wind speed values, with the fitted trend line predominantly influencing this correlation for lower W_S values. From Fig. 8, it might be concluded that ET_o values are higher for different wind speed values in low-wind conditions, where the influence of W_s on ET_o is more considerable. As wind speed increases, its impact on ET_o decreases.

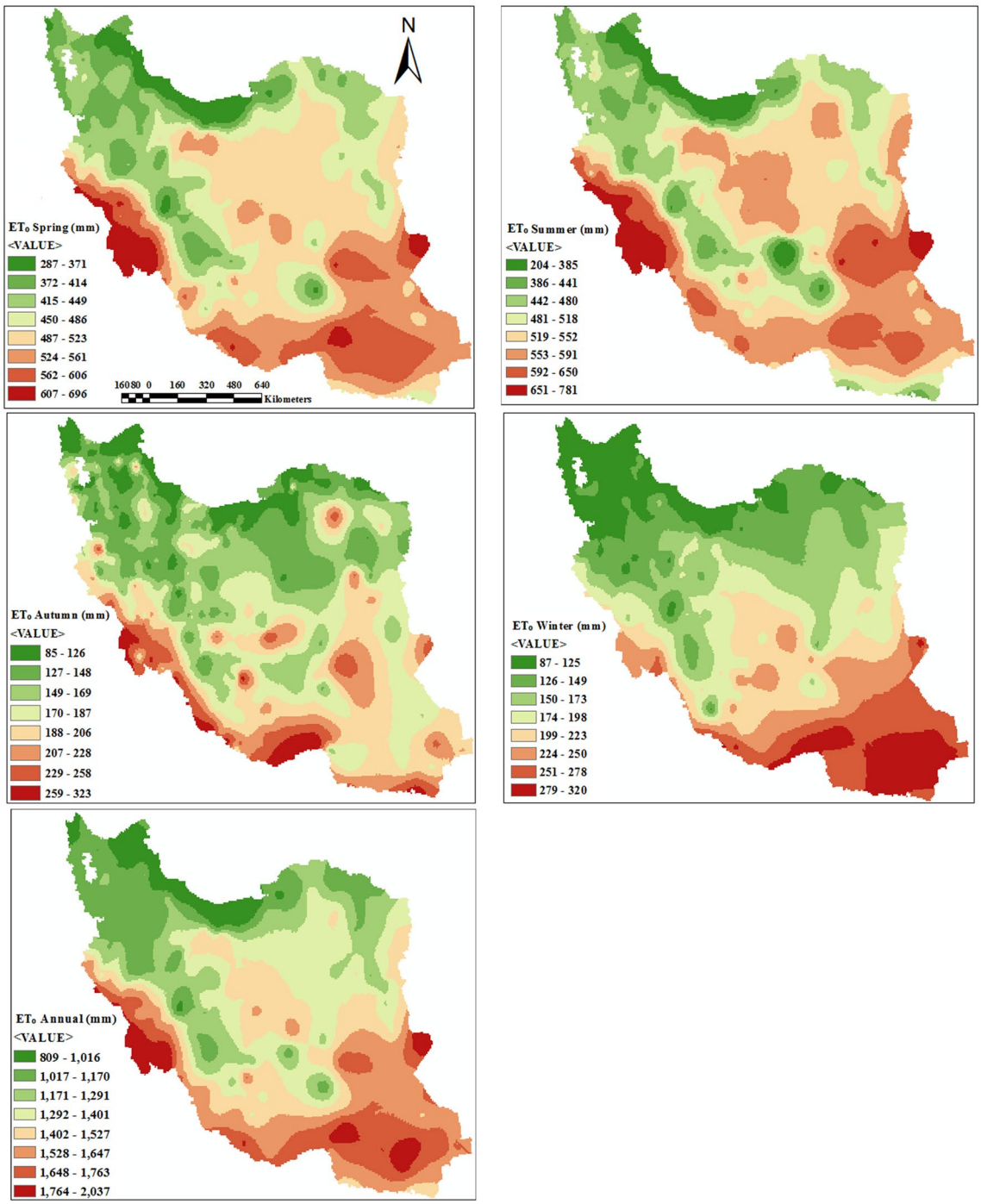

Fig. 6 Spatial distribution of seasonal and annual mean ET_o

Modeling spatial variations of ET_o

This section is focused on geographical processing with gridded (raster) data, interpolation, and modeling ET_o data from meteorological stations. OLS was applied that combines regression of the dependent variable (ET_o) on predictor/explanatory variables (such as elevation, latitude, air temperature). Before delving into the complexity of the new model, the first question would be, "Is it necessary to consider spatial dependence of the utilized data?" Here, the Moran's Index that is a spatial autocorrelation test was utilized to answer this question. Spatial autocorrelation is a powerful tool for examining the patterns of spatial self-correlation in data or residual models.

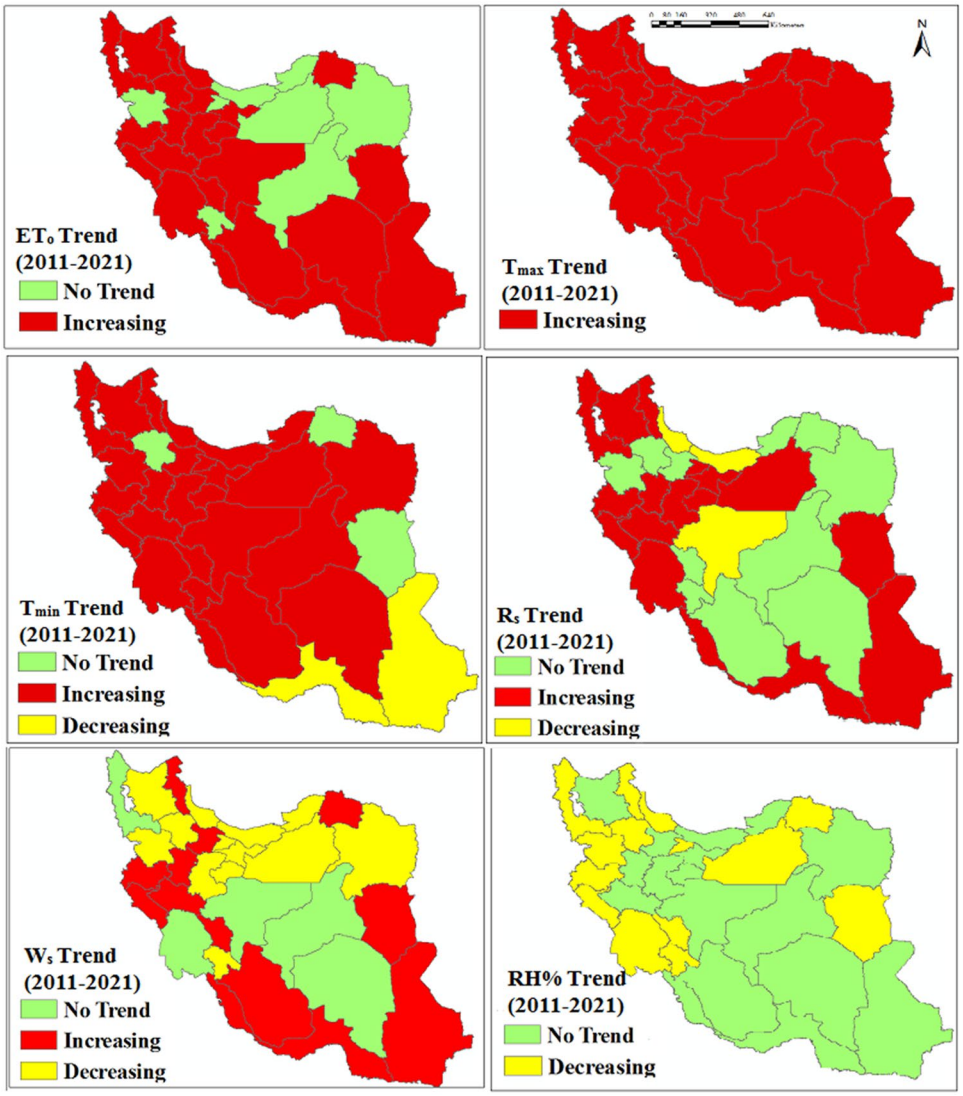

Fig. 7 Zoning of the time series trends of climatic variables from 2011 to 2021 (green points: no trend; yellow points: significant decreasing trends; red points: significant increasing trends)

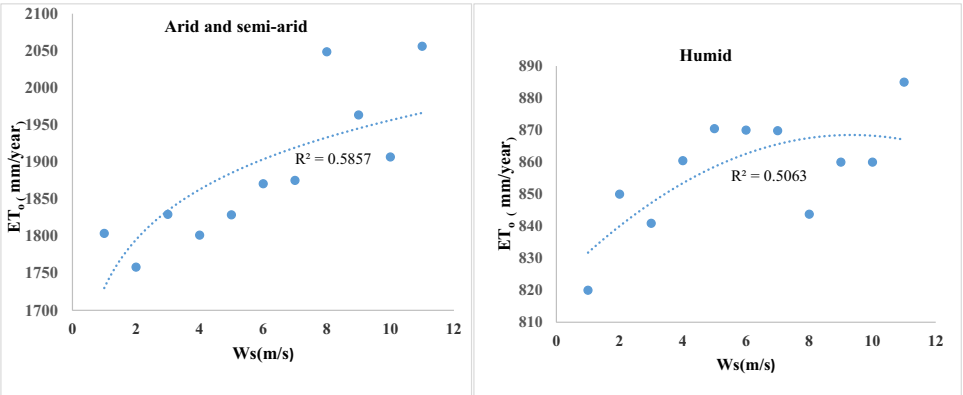

Fig. 8 Behavior of ET_o at different wind speed values

Figure 9 displays the spatial autocorrelation (S-AC) of ET_o values. The S-AC presents the degree of correlation between data when the distance between them is increased. While not as fundamental as variograms (geostatistics), they serve as useful exploratory and descriptive tools, as they provide better information than variograms. In this analysis (Fig. 9), the spatial residuals of the data are random or normal and acceptable, making the model reliable,

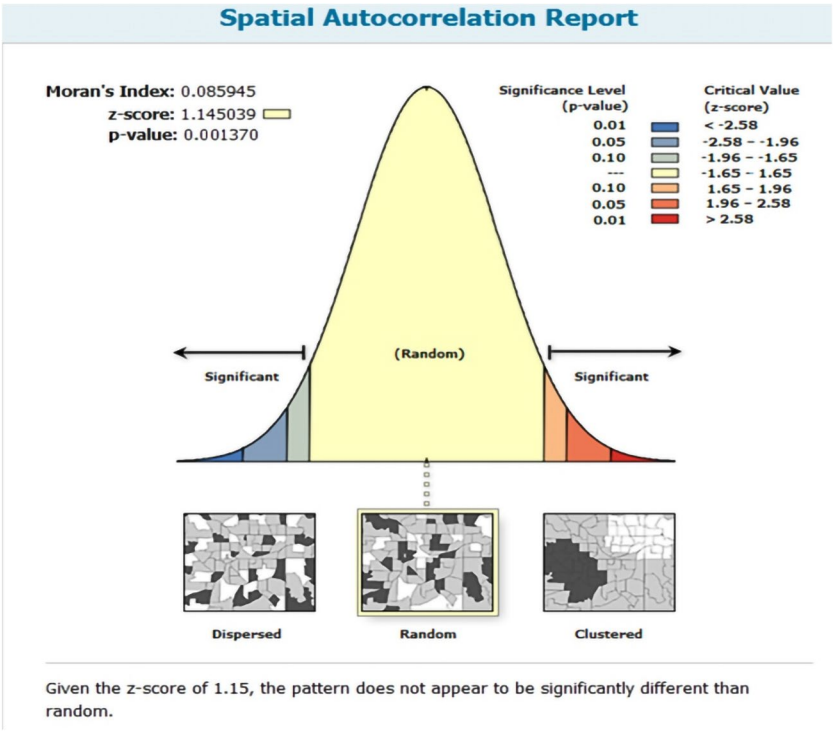

Fig. 9 Spatial autocorrelation of ET_o data

so the inclusion of other independent variables is no longer required. When the residuals of a regression-based model showed a scattered/clustered manner of distribution, this shows the model is incomplete/biased.

Sample data used for annual ET_o averages consist of six auxiliary variables considered candidates for modeling ET_o variations, i.e., elevation (m), geographical latitude (degrees), temperature changes (°C), solar radiation (MJ m^{-2} day^{-1}), wind speed at 2 m (ms^{-1}), and relative humidity (percentage). Figure 10 illustrates the merged raster map of ET_o combined with input parameters. A gridded layer for each predictor variable, with a spatial resolution of 0.009 degrees (approximately 1000 m) in the WGS geographic coordinate system, was created to calculate continuous surface values of ET_o in this figure.

Finally, by combining raster maps of solar radiation, wind speed, relative humidity, temperature changes, elevation, and geographical latitude, the least squares regression was applied to model ET_o. This modeling approach used both the elevation and geographical latitude maps to account for their effects, enhancing the model's accuracy. Table 4 displays the accuracy of the inputs for each model before introducing to the system. The best model was selected based on its performance, resulting in R^2 of 0.985, RMSE of 26.0, SI (normalized RMSE) of 0.021, and AICc of 318.0. Lower AICc values indicate a better and more efficient model. Additionally, the significance of the Jarque–Bera statistic suggests that the residuals exhibit

Fig. 10 The merged raster map of ET_o combined with input parameters

clustering behavior, so they are not random, indicating a need for more input variables.

Through the certainty of the input values of the OLS model, it is possible to predict the dependent variable, i.e., ET_o. For this purpose, the fitted regression line can be used.

Table 4 Summary of the results of the least squares regression method

Inputs	R^2	RMSE	SI	Jarque–Bera Statistic	Akaike's information criterion (AICc)	Variance inflation Factor (VIF)
R_s, W_s, RH%, ΔT, Altitude, Latitude	0.985	26	0.021	0.634193	318	VIF < 7.5
R_s, W_s, ΔT, Altitude, Latitude	0.97	39	0.03	0.686473	335	VIF < 7.5
R_s, ΔT, Altitude, Latitude	0.96	44	0.034	0.520025	338	VIF < 7.5
R_s, W_s, RH%, ΔT	0.812	96	0.076	0.000696*	386	VIF < 7.5
R_s, W_s, RH%, T_{max}, T_{min}, Altitude, Latitude	0.95	50	0.039	0.035791*	345	VIF < 7.5
R_s, W_s, Altitude, Latitude	0.93	55	0.043	0.003112*	342	VIF < 7.5
R_s, ΔT	0.8	98	0.076	0.016121*	377	VIF < 7.5

Variance inflation factor (VIF): large variance inflation factor (VIF) values (> 7.5) indicate redundancy among explanatory variables

Jarque–Bera Statistic: When this test is statistically significant ($p < 0.01$), model predictions are biased (the residuals are not normally distributed)

R-squared and Akaike's information criterion (AICc): Measures of model fit/performance

Figure 11 illustrates a comparison between observed and predicted ET_o by the selected model, demonstrating the high performance of the model with only slight deviations from the initial model. As observed in the scatterplot, ET_o has a strong positive correlation with air temperature and solar radiation, a weak positive correlation with wind speed, and a moderate negative correlation with relative humidity, elevation, and geographical latitude. Therefore, it can be concluded that solar radiation, daily temperature range, and humidity are among the primary factors contributing to ET_o variations.

Summary and conclusion

The present study aimed at the spatiotemporal interpolation ET_o in different climatic contexts of Iran. Data from 340 weather stations were utilized and some empirical techniques along with the ANN were applied for ET_o estimation.

At first, assessing the temporal (seasonal/annual) variations of the ET_o and relevant meteorological parameters during the study period across the country showed that the lowest ET_o values were observed in the humid and semi-humid climates in northern Iran, while higher ET_o values were observed in the arid and hyper-arid climates in the south, southeast, and east of the country. So, there is a clear upward trend in annual ET_o.

Then, the mutual information entropy was applied to analyze the information volume conveyed by each driven variable on target parameter (ET_o). Based on the results, the maximum air temperature conveys the highest information to ET_o followed by the minimum temperature, solar radiation, relative humidity, and wind speed.

Among the applied ET_o estimation models, the modified Hargreaves (MHGR) model showed the best fit in humid regions. The modified calibration coefficient of Hargreaves model was obtained as 0.213 (based on the analysis using data from 340 stations), which has been already recommended as 0.5 for Iran stations. Temperature-based BCR model was ranked as the second best model among other applied models. A comparison was also made between empirical equations and ET_o values obtained through remote sensing data (MODIS) that emphasized the superiority of MHGR model, although the Modis results were comparable and can be applied when no enough ground-based meteorological data are available in a region. Further, among various trained ANN models, the MLP model surpasses the rest of ANNs. Although the ANN fed with all necessary meteorological parameters outperformed the other ANN models, the accuracy reduction through excluding the other variables in temperature-based model was negligible, so the ANN with only temperature records as inputs might be suggested as a candidate of ET_o estimation through the region.

Finally, the spatial modeling of ET_o values using different techniques were performed and the annual/seasonal spatiotemporal variations were studied. Overall, the following most important concluding remarks were obtained here:

1- ET_o in Iran has mostly increased in all seasons and years over the past decade. This is mainly a result of continuous increases in air temperature in these regions. Since ET is the main factor affecting plant water requirements and considering that the agricultural sector is the largest consumer of water, changes in ET can have a significant impact on water balance.
2- Elevation plays a crucial role in estimating ET_o, as areas at higher elevations are less sensitive to temperature changes.

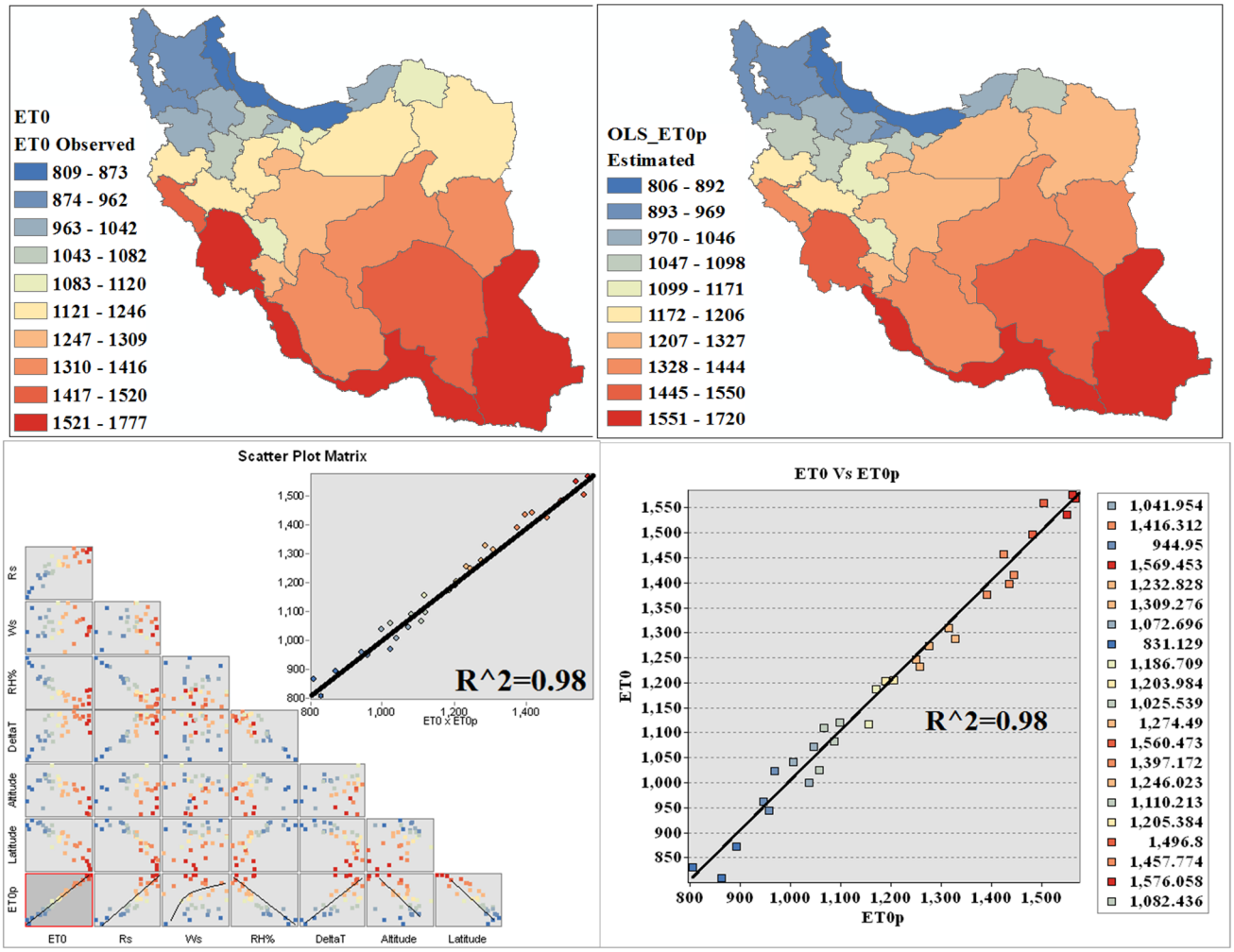

Fig. 11 Comparison of the OLS model with the FPM-56 method

3- The most significant changes have occurred in terms of relative humidity and temperature (obviously maximum and minimum temperatures). Air temperature is the most important meteorological factor influencing spatial and temporal changes in ET_o in these provinces.
4- Changes in ET_o have been attributed to variations in air temperature, net radiation, wind speed, and vapor pressure. Examining daily data, solar radiation, and air temperature have a positive effect on ET_o, while relative humidity, station elevation, and geographic latitude have a negative impact. Additionally, an increase in wind speed leads to an increase in ET_o in arid and semi-arid regions, whereas in humid areas, higher wind speeds result in reduction of ET_o.
5- For the entire basin, there is a significant upward trend in ET_o. A sudden spike in annual ET_o can be seen around 2016. Before 2016, ET_o decreased significantly, while after 2016, it increased rapidly. During 2011–2021, the dominant factors contributing to increased ET_o were reduced relative humidity and increased air temperature and solar radiation. The increase in wind speed also intensified ET_o up to a speed of 12 m per second in dry and semi-arid regions, beyond which, it plateaued and might reduce due to stomatal closure in plants. Wind speed had the opposite effect on ET_o in humid regions.
6- The highest values of ET_o are observed in the southwestern, southeastern, and eastern regions of the basin, while the lowest values are found in the northern and northwestern areas. This distribution pattern provides useful and valuable information for hydrological studies at the regional level because it is one of the most important determinants of regional ET_o, which in turn is a key parameter in the assessment of regional water resources and water management.
7- Southern, southeastern, and southwestern Iran experience higher ET intensities compared to the northern, northwestern, and northeastern regions, which can be attributed to the topography of the area. Therefore, high

ET and, consequently, increased aridity are inherent to these regions, making their ecosystems fragile.

8- The spatiotemporal dynamics of the four meteorological factors in this study are largely consistent with many studies on climate change. Wind speed has significantly decreased in northern, northwestern, and northeastern regions of Iran, possibly due to the weakening of the Asian monsoon system. Conversely, regional wind intensification may be attributed to an increase in local wind systems.

9- Relative humidity has significantly decreased. Most areas belong to the arid region, and water resources are limited. Increased air temperature leads to higher saturation vapor pressure, which may be the reason for decreased RH (It is consistent with the results of Chen et al., 2006). Climatic factors and ET_o have complex interdependencies, and among them, sudden changes in ET_o can occur.

10- A minor decreasing trend in solar radiation (R_s) was observed in the northern regions of Iran during 2011–2021, possibly due to increased water vapor and cloud cover. The lowest R_s is observed in the Caspian Sea region and the mountainous northwestern areas of Iran, while higher R_s values are observed in predominantly arid regions. In the southeast, central, and eastern regions, it can be inferred that R_s increases with clear skies controlled by geographic latitude and elevation. R_s also increases in windy locations, as observed in the southeastern and eastern parts of Iran.

Overall, the comprehensive analysis of these results indicates that the climate in the region will become warmer and drier in the coming years. The rising air temperatures and subsequent increase in ET_o indicate the prevalence of climatic changes in our region. It is imperative that we prepare for these new climatic conditions, which may bring about alterations in rainfall patterns, as well as fluctuations in the growth periods of plants across different regions. This could lead to instances of drought, flooding, and other factors that may significantly impact agricultural performance. Over the long term, these changes have the potential to make certain areas wetter while rendering others drier, thereby exposing us to the risk of water stress.

Author contribution All authors contributed to the study conceptualization. Material preparation and data analysis were performed by *Mostafa Sadeghzadeh*. Study conceptualization and supervision was performed by *Jalal Shiri*. Modeling and interpretation were performed by *Mostafa Sadeghzadeh* and *Sepideh Karimi*. *Mostafa Sadeghzadeh* and *Jalal Shiri* prepared the preliminary draft of the paper. *Abolfazl Majnooni* contributed to results analysis and draft review. All authors read and commented on the paper draft and approved the final version.

Data availability Data will be available per request.

Declarations

Ethical approval Accepted principles of ethical and professional conduct have been followed.

Consent to participate The authors confirm that any participants, who may be identifiable through the manuscript, have been given an opportunity to review the final manuscript and have provided written consent to publish.

Consent to publish Not applicable.

Competing interests The authors declare no competing interests..

References

Abraham M, Mohan S (2023) ANN-based PCA to predict evapotranspiration: a case study in India. AQUA—Water Infrastruct Ecosyst Soc 72(7):1145–1163

Allen RG, Pereira LS, Raes D, Smith M (1998) Crop evapotranspiration-guidelines for computing crop water Requirements-FAO Irrigation and Drainage Paper 56. 9th edn. Food Agric Organ U N: Rome. Italy

Allen RG, Tasumi M, Trezza R (2007) Satellite-based energy balance for mapping evapotranspiration with internalized calibration (METRIC)-Model. J Irrig Drain Eng 133(4):380–394

Bastiaanssen WGM (2000) SEBAL-based sensible and latent heat fluxes in the irrigated Gediz Basin, Turkey. J Hydrol 229(1–2):87–100. https://doi.org/10.1016/S0022-1694(99)00202-4

Bednarik M, Magulova B, Matys M, Marschalko M (2010) Landslide susceptibility assessment of the Kral ovany–Liptovsky Mikulas railway case study. J Phys Chem Earth 35(3–5):162–171

Beven K (2006) A manifesto for the equifinality thesis. J Hydrol 320(1–2):18–36

Blaney H, Criddle W (1950) Determining water needs from climatological data. USDA Soil Conserv Serv. SOS–T.P. USA. p 8–9

Bogawski P, Bednorz E (2014) Comparison and validation of selected evapotranspiration models for conditions in Poland (Central Europe). Water Resour Manage 28:5021–5038

Burn DH, Hesch NM (2007) Trends in evaporation for the Canadian Prairies. J Hydrol 336:61–73

Chen S, Liu Y, Axel T (2006) Climatic change on the Tibetan Plateau: potential evapotranspiration trends from 1961–2000. Clim Chang 76:291–319

Chu R, Li M, Shen S, Islam ARMT, Cao W, Tao S, Gao P (2017) Changes in reference evapotranspiration and its contributing factors in Jiangsu, a major economic and agricultural province of eastern China. Water 9:486

Chuanyan Z, Zhongren N, Guodong C (2005) Methods for modelling of temporal and spatial distribution of air temperature at landscape scale in the southern Qilian mountains. China Ecol Model 189:209–220

Coulibaly P, Anctil F, Aravena R, Bobée B (2001) Artificial neural network modeling of water table depth fluctuations. Water Resour Res 37:885–896

Dadaser-Celik F, Cengiz E, Guzel O (2015) Trends in ET_o in Turkey: 1975–2006. Int J Climatol 38:S83

Dobesch H, Dumolard P, Dyras I (eds) (2007) Spatial interpolation for climate data: the use of gis in climatology and meteorology. London, ISTE Ltd

Doorenbos J, Pruitt WO (1977) Guidelines for predicting crop water requirement. Irrigation and Drainage Paper 24, 2nd edn. Food Agriculture Organization of the United Nation, Rome.

Gianniou SK, Antonopoulos VZ (2007) Evaporation and energy budget in Lake Vegoritis. Greece J Hydrol 345:212–223

Glenn EP, Huete AR, Nagler PL, Nelson SG (2008) Relationship between remotely sensed vegetation indices, canopy attributes and plant physiological processes: what vegetation indices can and cannot tell us about the landscape. Sensors 8(4):2136–2160. https://doi.org/10.3390/s8042136

Glenn EP, Nagler PL, Huete AR (2010) Vegetation index methods for estimating evapotranspiration by remote sensing. Surv Geophys 31(6):531–555. https://doi.org/10.1007/s10712-010-9102-2

Gong L, Yu C, Chen D, Halldin S, Chen Y (2006) Sensitivity of the Penman-Monteith reference evapotranspiration to key climatic variables in the Changjiang (Yangtze River) basin. Hydrology 329:620-629

Goovaerts P (1997) Geostatistics for natural resources evaluation. Oxford University Press, New York

Goulden M, Anderson R, Bales R, Kelly A, Meadows M, Winston G (2012) Evapotranspiration along an elevation gradient in California's Sierra Nevada. J Geophys Res 117(G3):G03036

Goyal R (2004) Sensitivity of evapotranspiration to global warming: a case study of arid zone of Rajasthan (India). Agric Water Manag 69(1):11

Hamed KH, Rao AR (1998) A modified Mann-Kendall trend test for autocorrelated data. J Hydrol 204(1–4):182–196

Hargreaves GH, Samani ZA (1985) Reference crop evapotranspiration from temperature. Trans. ASAE 1(2):96–99

Intergovernmental Panel on Climate Change (IPCC) (2014) Climate Change., 2014. Synthesis report. In: Pachauri RK, Meyer LA (eds). In contribution of working groups I, II and III to the fifth assessment report of the intergovernmental panel on climate change. Core writing team; IPCC: Geneva, Switzerland p 151

Irmak S, Mutiibwa D (2009) On the dynamics of stomata resistance: relationships between stomata behavior and micrometeorological variables and performance of Jarvis-type parameterization. Trans ASABE 52(6):1923–1939

Irmak S, Payero J, Martin DL, Irmak A, Howell TA (2006) Sensitivity analysis and sensitivity coefficients of standardized daily ASCE-Penman-Monteith equation. Am Soc Civil Eng 132(6):564–578

Jain SK, Nayak PC, Sudheer KP (2008) Models for estimating evapotranspiration using artificial neural networks, and their physical interpretation. Hydrol Process 22:2225–2234

Jhajharia D, Dinpashoh Y, Kahya E, Singh VP, Fakheri-Fard A (2012) Trends inreference evapotranspiration in the humid region of northeast India. J Hydrol 26:421–435

Kun Y, Baohong D, Jun Q, Wenjun T, Ning L, Changgui L (2012) Can aerosol loading explain the solar dimming over the Tibetan Plateau? Geophys Res Lett 39:L20710

Lawrimore JH, Peterson TC (2000) Pan evaporation trends in dry and humid regions of the United States. J Hydrometeorol 1:543–546

Li ZL, Tang RL, Wan ZM, Bi YY, Zhou CH, Tang BH, Yan GJ, Zhang XY (2009) A review of current methodologies for regional evapotranspiration estimation from remotely sensed data. Sensors 9(5):3801–3853. https://doi.org/10.3390/s90503801

Liu C, Zhang D (2011) Temporal and spatial change analysis of the sensitivity of potential evapotranspiration to meteorological influencing factors in China. Acta Geogr Sin 66:579–588

Liu H, Zhang R, Li Y (2014) Sensitivity analysis of ET_o to climate change in Beijing, China. Desalin Water Treat 52:2799–2804

Lu X, Zang C, Burenina T (2020) Study on the variation in evapotranspiration in different period of the Genhe River Basin in China. Phys Chem Earth 120:102902

Maeda EE, Wiberg DA, Pellikka PKE (2011) Estimating ETo using remote sensing and empirical models in a region with limited ground data availability in Kenya. Appl Geogr 31:251–258

Mogheir Y, Singh VP (2003) Specification of information needs for groundwater management planning in developing country. Groundw Hydrol 2:3–20

Mu Q, Zhao M, Running SW (2011) Improvements to a MODIS global terrestrial evapotranspiration algorithm. Remote Sens Environ 115(8):1781–1800. https://doi.org/10.1016/j.rse.2011.02.019

Niggli U, Fließbach A, Hepperly P, Scialabba N (2009) Low greenhouse gas agriculture: mitigation and adaptation potential of sustainable farming systems. Ökol Landbau 141:32–33

Patle GT, Singh DK (2015) Sensitivity of annual and seasonal reference crop evapotranspiration to principal climatic variables. Earth Syst Sci 124(4):819–828

Penman HL (1948) Natural evaporation from open water, bare soil and grass. Proc R Soc Lond 193:120–145

Raziei T, Pereira LS (2013) Spatial variability analysis of ET_o in Iran utilizing fine resolution gridded datasets. Agric Water Manag 126:104–118

Schuur E, McGuire A, Schädel C, Grosse G, Harden J, Hayes D, Hugelius G, Koven C, Kuhry P, Lawrence D (2015) Climate change and the permafrost carbon feedback. Nature 520:171–179

Shahid S (2011) Impact of climate change on irrigation water demand of dry season Boro rice in northwest Bangladesh. Clim Change 105(3):433–453

Shannon CE, Weaver W (1949) The mathematical theory of communication. Urbana IL Univ Illinois Press 1(117):39

Shiri J (2018) Improving the performance of the mass transfer-based reference evapotranspiration estimation approaches through a coupled wavelet-random forest methodology. J Hydrol 561:737–750

Shiri J (2019) Modeling reference evapotranspiration in island environments: assessing the practical implications. J Hydrol 570:265–280

Shiri J, Sadraddini AA, Nazemi AH, Kisi O, Landeras G, Fard AF, Marti P (2014) Generalizability of gene expression programming-based approaches for estimating daily ET_o in coastal stations of Iran. J Hydrol 508:1–11

Shiri J, Sadraddini AA, Nazemi AH, Marti P, Fard AF, Kisi O, Landeras G (2015) Independent testing for assessing the calibration of the Hargreaves–Samani equation: New heuristic alternatives for Iran. Comput Elec Agric 117:70–80

Stephen MS (1981) Gauss and the invention of least squares. Ann Stat 9(3):465–474. https://doi.org/10.1214/aos/1176345451

Subburayan S, Murugappan A, Mohan S (2011) Modified Hargreaves equation for estimation of ET_o in a hot and humid location in Tamilnadu State. India Int J Eng Sci Technol 3(1):592–600

Tong L, Kang S, Zhang L (2007) Temporal and spatial variations of evapotranspiration for spring wheat in the Shiyang river basin in northwest China. Agric Water Manag 87:241–250

Traore S, Luo Y, Fipps G (2016) Deployment of artificial neural network for short-term forecasting of evapotranspiration using public weather forecast restricted messages. Agric Water Manage 163:363–379

UNEP (1992) World Atlas of Desertification. In: Edward Arnold, London

Vicente-Serrano SM, Azorin-Molina C, Sanchez-Lorenzo A, Revuelto J, Morán-Tejeda E, López-Moreno JI, Espejo F (2015) Sensitivity of ET_o to changes in meteorological parameters in Spain (1961–2011). Water Resour Res 50:8458–8480

Wu W, Dandy GC, Maier HR (2014) Protocol for developing ANN mode ls and its application to the assessment of the quality of the ANN model development process in drinking water quality modelling. Environ Model Softw 54:108–127

Zhang Z, Yang Y, Zhang X, Chen Z (2014) Wind speed changes and its influencing factors in Southwestern China. Acta Ecol Sin 34:471–481

Zhang L, Zhang J, Traore S, Je G, Zhao X, Zhan H, Singh VP (2022) Continental-scale spatiotemporal calibration of the Blaney-Criddle equation for different climate zones in China. Journal of Hydrology: Regional Studies 44:101233

Zheng C, Wang Q (2015) Spatiotemporal pattern of the global sensitivity of the ET to climatic variables in recent five decades over China. Stoch Environ Res Risk Assess 29:1937–1947